Alzheimer's & Dementia: Diagnosis, Assessment & Disease Monitoring ■ (2015) 1-10

Alzheimer's & Dementia

Prediction of Alzheimer's disease pathophysiology based on cortical thickness patterns

Q1

Q10 Jihye Hwang[a], Chan Mi Kim[a,b], Seun Jeon[c], Jong Min Lee[c], Yun Jeong Hong[a], Jee Hoon Roh[a,d,*], Jae-Hong Lee[a], Duk L. Na[e,f], and Alzheimer's Disease Neuroimaging Initiative[1]

[a]Department of Neurology, Asan Medical Center, University of Ulsan College of Medicine, Seoul, Korea
[b]Department of Medical Engineering, Asan Medical Center, University of Ulsan College of Medicine, Seoul, Korea
[c]Department of Biomedical Engineering, Hanyang University, Seoul, Korea
[d]Department of Anatomy and Cell Biology, Cell Dysfunction Research Center (CDRC), University of Ulsan College of Medicine, Seoul, Korea
Q2 [e]Department of Neurology, Samsung Medical Center, School of Medicine, Sungkyunkwan University
[f]Neuroscience Center, Samsung Medical Center

Abstract

Introduction: Recent studies have shown that pathologically defined subtypes of Alzheimer's disease (AD) represent distinctive atrophy patterns and clinical characteristics. We investigated whether a cortical thickness–based clustering method can reflect such findings.

Methods: A total of 77 AD subjects from the Alzheimer's Disease Neuroimaging Initiative 2 data set who underwent 3-T magnetic resonance imaging, [^{18}F]-fluorodeoxyglucose-positron emission tomography (PET), [^{18}F]-Florbetapir PET, and cerebrospinal fluid (CSF) tests were enrolled. After clustering based on cortical thickness, diverse imaging and biofluid biomarkers were compared between these groups.

Results: Three cortical thinning patterns were noted: medial temporal (MT; 19.5%), diffuse (55.8%), and parietal dominant (P; 24.7%) atrophy subtypes. The P subtype was the youngest and represented more glucose hypometabolism in the parietal and occipital cortices and marked amyloid-beta accumulation in most brain regions. The MT subtype revealed more glucose hypometabolism in the left hippocampus and bilateral frontal cortices and less performance in memory tests. CSF test results did not differ between the groups.

Discussion: Cortical thickness patterns can reflect pathophysiological and clinical changes in AD.

Keywords: Alzheimer's disease; Cortical thickness; Alzheimer's Disease Neuroimaging Initiative; Magnetic resonance imaging; Positron emission tomography

1. Background

Aggregations of amyloid-beta (Aβ) and tau protein are the two main pathologic hallmarks of Alzheimer's disease (AD). Although the aggregation of Aβ is known to precede the tau pathology in AD, the earlier role of tau aggregation in the pathogenesis of AD and aging has been reemphasized [1,2]. The accumulation of tau has been noted in the transentorhinal cortices with normal aging and such tau aggregation is known to accelerate the spread of Aβ pathology in the AD brain [1–3]. Moreover, the accumulation of tau proteins correlates very closely with cognitive decline and brain atrophy including hippocampal atrophy [4,5]. Hence, defining AD based on the tau pathology in the brain would enable a better understanding of the clinical implications of tau accumulation in this disease.

Recently, neuropathologically defined subtypes of AD have represented distinctive clinical characteristics and brain structural changes such as (1) typical generalized

The investigators within the ADNI contributed to the design and implementation of ADNI and/or provided data but did not participate in analysis or writing of this report. The authors declare no conflicts of interest in relation to this study.

[1]All the data used in preparation of this article were obtained from the ADNI database (http://adni.loni.usc.edu). A complete listing of ADNI investigators can be found at: http://adni.loni.usc.edu/wp-content/uploads/how_to_apply/ADNI_Acknowledgement_List.pdf.

*Corresponding author. Tel.: +82-2-3010-3443; Fax: +82-2-474-4691.
E-mail address: roh@amc.seoul.kr; alzheimer@naver.com (J.H.R.)

http://dx.doi.org/10.1016/j.dadm.2015.11.008

atrophy involving medial temporal (MT) lobes; (2) limbic predominant atrophy; (3) and hippocampus-sparing atrophy [6,7]. Because pathologic assessment cannot be easily applied to most of AD subjects in vivo, our group recently investigated whether clustering of AD subjects based on magnetic resonance imaging (MRI) cortical thickness patterns can replicate autopsy-based findings. Interestingly, the MRI cortical thickness pattern–based clustering was comparable with the autopsy-based classification of AD in an earlier report [8]. However, there was no assessment in that previous study as to whether the new clustering method based on cortical thickness patterns can also reflect pathophysiological changes in AD. If so, this would potentially provide additional clinical information on structural brain magnetic resonance (MR) images and, thus, further knowledge of the underlying pathogenesis as well as prognosis of the disease.

We investigated whether the new cortical thickness–based clustering methodology could be replicated in a multicenter, international data set. We also sought to determine whether this clustering method reflected the pathophysiological status of AD as assessed by [^{18}F]-fluorodeoxyglucose (FDG)-positron emission tomography (PET), [^{18}F]-Florbetapir PET, and cerebrospinal fluid (CSF) Aβ and tau protein tests.

2. Methods

2.1. Participants

Data used for the preparation of this article were obtained from the Alzheimer's Disease Neuroimaging Initiative (ADNI) database (adni.loni.usc.edu). The ADNI is described in Supplemental Methods. We selected 89 AD subjects from the ADNI-2 study who had high-resolution 3-T T1-weighted MRI, baseline FDG-PET, baseline Florbetapir-PET, and available baseline CSF results. Among these 89 subjects, 12 cases were excluded because of segmentation errors in MRI cortical thickness analysis and a total of 77 subjects were included for analyses. For comparison and to obtain representative MR images of each group, we also used data from 42 subjects with normal cognition in the ADNI-2 who underwent the baseline imaging and CSF studies and remained normal at 2-year follow-up assessments.

2.2. Image analysis

2.2.1. MRI analysis

2.2.1.1. MRI acquisition

We followed ADNI procedure in our current analysis. Briefly, we used screening 3-T T1-weighted MRI sequence with rapid gradient echo (MPRAGE) images with a 1.2-mm-slice thickness. Subjects who underwent 1.5 T MRI or MRI sequence with enhanced spoiled gradient were not included because of greater signal-to-noise ratio or less compatibility between sequences. All data were downloaded from LONI (as of October 2014). Additional details regarding data acquisition are available elsewhere (http://www.adni-info.org).

2.2.1.2. Measurements of cortical thickness

The cortical thickness of the initial cohort of 89 AD subjects was measured as described previously [9]. Three-Tesla T1-weighted MRI images were processed using a standard Montreal Neurological Institute (MNI) anatomic pipeline (version 1.1.9; http://wiki.bic.mni.mcgill.ca/index.php/CIVET). We registered all native volumetric T1 images into a standardized stereotaxic space using a linear transformation [10]. An N3 algorithm was used to correct for intensity non-uniformities using inhomogeneities in the magnetic field [11]. The corrected volumetric images were then classified into white matter, gray matter (GM), CSF, and background using an Intensity-Normalized Stereotaxic Environment for Classification of Tissues algorithm [12]. The surfaces of the inner and outer cortices were automatically extracted using a Constrained Laplacian-Based Automated Segmentation with Proximities algorithm [13]. Finally, the Euclidean distances between linked vertices on the inner and the outer surface were calculated for the cortical thickness measurement [14].

2.2.1.3. Cluster analyses

We performed hierarchical agglomerative cluster analysis using Statistics and Machine Learning Toolbox implemented in MATLAB version 8.2.0.29 R2013b (MathWorks, Natick, MA, USA) in which each patient begins in his or her own cluster and at each step the two most "similar" clusters are combined until the last two clusters are combined into a single cluster with all patients. We used the whole-brain cortical thickness for the clustering: a total of 78,570 vertex points (without noncortical regions) for each of the 77 AD subjects. To cluster patients according to the thinning patterns of each cortical region, rather than a global atrophy, the variations in global atrophy between patients were compensated for by normalizing the cortical thickness values from vertices to a mean cortical thickness [15]. The Ward's clustering linkage method [15,16] was used to combine pairs of clusters. The clustering begins with each patient in his or her own cluster (n = 77, size 1 each). At each step, the Ward's method chooses which pair of clusters to be combined next by merging the pair of clusters while minimizing the sum of square errors (the two most similar clusters) from the cluster mean. For instance, n-1 clusters are formed in the first step (one cluster of size 2). Then, n-2 clusters are formed in the second step (two clusters of size 2 or one cluster of size 3 including the cluster formed in step 1). The algorithm continues until all patients are merged into a single large cluster (size n). Finally, each of the 77 AD patients was placed in their own cluster and then progressively clustered with others. The cluster analysis results are shown as a dendrogram (Fig. 1).

2.2.2. PET analyses

2.2.2.1. PET acquisition

We followed the ADNI procedure, and data were downloaded (as of October 2014) from LONI in the processed format (series description in LONI Advanced Search: AV45 co-registered and averaged; and FDG co-registered and averaged). The details of the acquisition are available at http://www.adni-info.org.

2.2.2.2. PET analyses

To analyze the Florbetapir- and FDG-PET images, the skull was stripped and the brain was extracted using a FMRIB software library. We then automatically co-registered the PET image for each subject to the corresponding skull-stripped MR image using a rigid-body registration method. These co-registered images were spatially normalized to a MNI atlas space. The partial volume correction was performed using results with more than 25% of the maximal regional intensity [17]. The mean standard uptake value ratio (SUVr) in the cerebellum GM was used as a reference. The cortex-to-cerebellum regional SUVr for 78 regions of interest of automated anatomical labeling template were finally calculated for comparison between groups.

2.3. CSF analyses

CSF acquisition and biomarker measurements using the ADNI cohort were performed as previously described and as per the ADNI procedure [18].

2.4. Statistical analyses

Group analyses were performed using SPSS software (version 22.0; SPSS Inc, Chicago, IL, USA) and R (version 3.2.2). We used a one-way analysis of variance test to compare age, education, and intracranial volume (ICV) and a χ^2 test to compare sex. We used the analysis of covariance (ANCOVA) test to compare the other demographic characteristics and neuropsychological test results, with age, sex, education, and ICV serving as covariates. Between-group comparisons of the continuous variables were performed using ANCOVA and logistic regression for categorical variables (e.g., APOE and clinical dementia rating [CDR]). We used the Kruskal-Wallis test for variables not fulfilling a normal distribution. Cortical thickness analyses were performed using a linear modeling method for the thickness maps after controlling for the mean cortical thickness. To avoid false positives, resulting statistical maps satisfying a false discovery rate (FDR) correction at a 0.05 significance level were determined [19]. For direct comparison of the SUVr of each cortical region of interest of FDG-PET and Florbetapir-PET, we performed ANCOVA test with age, sex, education, and ICV serving as covariates. Multiple comparisons among three groups at FDR corrected $P < .05$ were considered statistically significant. For comparison of CSF results, ANCOVA was performed with age, sex, education, and ICV serving as covariates. Phosphorylated-tau (p-tau) and p-tau/Aβ data were log transformed before the analysis [18].

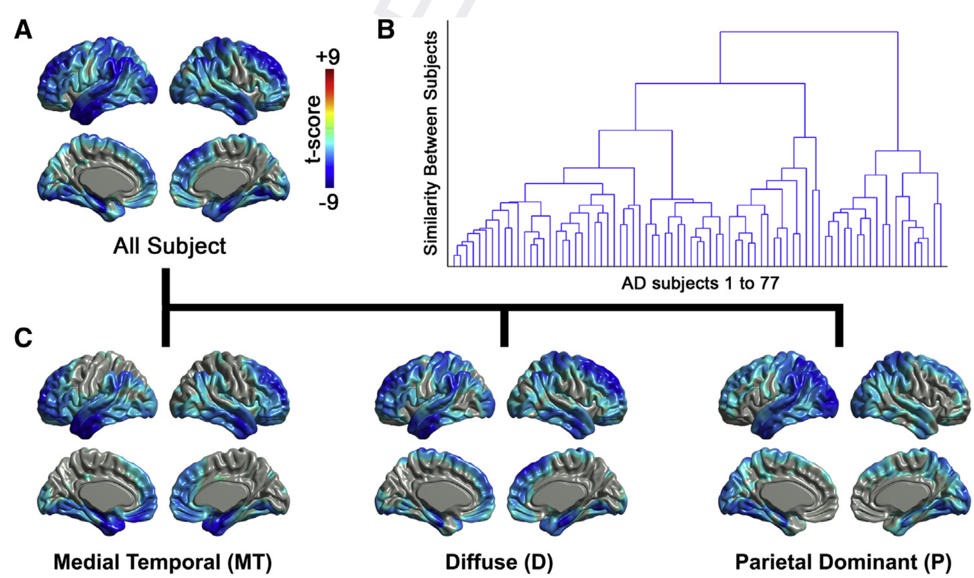

web 4C/FPO

Fig. 1. Dendrogram and representative figures for the three AD subtypes. (A) A representative figure of cortical thickness patterns of all 77 subjects with AD compared with 42 subjects with normal cognition. The scale bar indicates the T-value from −4.0 to 4.0 with bluish color representing more cortical thinning in AD patients compared with normal subjects. Gray areas indicate brain regions showing no statistical significance in cortical thickness compared with normal control groups. (B) Dendrogram created by cluster analysis based on cortical thickness patterns used to obtain three representative cortical thinning subtypes in AD. (C) Representative images of the cortical thinning patterns in the three subtypes of AD compared with 42 subjects with normal cognition. Abbreviation: AD, Alzheimer's disease.

3. Results

All 77 AD study subjects were clustered into three subtypes, and the cortical thinning patterns in each of the three AD subtypes were shown in comparison with 42 cognitively normal controls (Fig. 1). The three subtypes include (1) MT subtype (n = 15, 19.5%), in which the bilateral MT lobes were predominantly involved with the additional involvement of the bilateral frontal lobes; (2) D subtype (n = 43, 55.8%), in which nearly all association cortical areas such as the bilateral dorsolateral frontal lobes, lateral temporal, and lateral parietal lobes were affected; and (3) parietal dominant subtype (P subtype, n = 19, 24.7%), in which the bilateral lateral parietal lobes, and some bilateral occipital lobes were affected with little involvement of MT lobes (Fig. 1A).

The demographics and clinical characteristics of each subtype were found to differ (Table 1). Patients in the P subtype (mean years [±standard deviation {SD}], 67.53 [±7.35]) were younger than the other two subtypes (MT subtype, 74.8 [±7.88]; D subtype, 76.05 [±6.56]; P = .0002). The P subtype was suggestive of early-onset Alzheimer's disease (EOAD) with younger age at symptom onset than the other two subtypes (MT subtype, mean [±SD] age at onset = 69.87 years [±8.19]; D subtype, 70.95 years [±7.12]; P subtype, 63.47 years [±7.78]; P = .002). There were no statistically significant differences in sex, education level, ICV, APOE status, and global cognitive function measured by mini-mental state examination (MMSE) score, CDR, clinical dementia rating scale-sum of boxes (CDR-SB), Alzheimer's disease assessment scale-cognitive subscale (ADAS-Cog) 11, ADAS-Cog 13, Montreal cognitive assessment (MoCA), and geriatric depression scale (GDepS).

In FDG-PET analysis, all groups showed a significant difference in glucose hypometabolism in the different regions, corresponding to cortical thinning patterns (Table 2 and Fig. 2B). Patients in the P subtype showed glucose hypometabolism in the right superior, left inferior parietal, and left middle occipital cortices. Patients in the MT subtype showed glucose hypometabolism in the left hippocampus, left inferior orbital frontal, right superior medial frontal, and both caudate areas. Differences in the Florbetapir-PET results were most prominent in the P subtype patients (Table 3, Fig. 3) who showed marked Aβ accumulation in the superior, middle, and inferior frontal cortex, superior and inferior parietal cortex, and precuneus compared with that in the MT and D subtypes. Patients in the MT subtype had more Aβ accumulation in the left precuneus and right mesial frontal cortex compared with that in the D subtype (Fig. 3). In neuropsychological battery analysis (Table 4), MT subtype showed a lower ADNI-MEM score than the D subtype (MT subtype = −0.80 [±0.41]; D subtype −0.44 [±0.44], P = .0237). P subtype showed a longer trail making test-A time (MT subtype, mean [±SD] age = 55.07 [±28.39]; D subtype, 58.95 [±34.22]; P subtype, 80.67 [±39.46]; P = .0412) and a lower performance in interlocking pentagon task than the other two subtypes (MT subtype, 86.7%; D subtype, 88.4%; P subtype, 21.1%; P < .0001). The CSF results showed no statistically significant differences between the subtypes (Supplemental Table 1).

Table 1
Demographics and clinical characteristics Q7

Characteristics	MT subtype (n = 15)	D subtype (n = 43)	P subtype (n = 19)	P	Adjusted P
Age, y (mean ± SD)	74.8 ± 7.88	76.05 ± 6.56	67.53 ± 7.35	.0002*†	
Women, n (%)	7 (46.67)	18 (41.86)	9 (47.37)	.9004	
Education, y (mean ± SD)	15.67 ± 3.06	16.16 ± 2.35	15.53 ± 2.50	.6085	
Age at onset, y (mean ± SD)	69.87 ± 8.19	70.95 ± 7.12	63.47 ± 7.78	.002*†	
ICV, cm^3 (mean ± SD)	1.31 ± 0.18	1.32 ± 0.16	1.28 ± 0.15	.7129	
Mean cortical thickness	3.00 ± 0.13	3.07 ± 0.14	3.01 ± 0.18	.189	.137
ApoE4 allele, n (%)	10 (66.67)	31 (72.09)	13 (68.42)	.9767	.94
MMSE, (mean ± SD)	22.60 ± 1.99	23.51 ± 1.99	22.74 ± 2.28	.2151	.275
CDR, n (%)				.6785	.577
0.5	7 (46.67)	21 (48.84)	7 (36.84)		
≥1	8 (53.33)	22 (51.16)	12 (63.16)		
CDR-SB, (mean ± SD)	4.43 ± 1.84	4.55 ± 1.65	4.16 ± 1.38	.6885	.6421
ADAS-Cog 11, (mean ± SD)	21.93 ± 7.50	19.38 ± 6.41	22.95 ± 8.06	.1542	.5288
ADAS-Cog 13, (mean ± SD)	31.87 ± 8.95	28.19 ± 9.91	34.00 ± 9.24	.0762	.4903
MoCA (mean ± SD)	16.80 ± 4.80	17.35 ± 4.37	16.67 ± 5.63	.8513	.9812
GDepS, (mean ± SD)	1.20 ± 0.94	1.49 ± 1.44	1.53 ± 0.84	.6949	.7456

Abbreviations: MT subtype, medial temporal subtype; D subtype, diffuse atrophy subtype; P subtype, parietal-dominant subtype; SD, standard deviation; ICV, intracranial volume; APOE, apolipoprotein E; MMSE, mini-mental state examination; CDR, clinical dementia rating scale; CDR-SB, clinical dementia rating scale-sum of boxes; ADAS-Cog 11, Alzheimer's disease assessment scale-cognitive subscale 11; ADAS-Cog 13, Alzheimer's disease assessment scale-cognitive subscale 13; MoCA, Montreal cognitive assessment; GDepS, geriatric depression scale.

NOTE. For each variable, the mean and standard deviation were shown. Age, gender, education, and ICV were treated as covariates in the analysis of APOE, MMSE, GDepS, ADAS-Cog 13, CDR, and CDR-SB.

*P < .05 between MT subtype and P subtype.

†P < .05 between D subtype and P subtype.

Table 2
Glucose metabolism of each region of interest of FDG-PET

	MT subtype (n = 15)	D subtype (n = 43)	P subtype (n = 19)	
Region of interest	Mean ± SD	Mean ± SD	Mean ± SD	Adjusted *P*
Inferior orbital frontal, Lt	0.81 ± 0.05	0.86 ± 0.08	0.89 ± 0.06	.0113*†
Superior medial frontal, Rt	0.85 ± 0.04	0.89 ± 0.08	0.93 ± 0.07	.0293*†
Hippocampus, Lt	0.71 ± 0.06	0.76 ± 0.06	0.76 ± 0.06	.0144*
Middle occipital, Lt	1.05 ± 0.07	1.03 ± 0.11	0.97 ± 0.12	.0223†‡
Superior parietal, Rt	0.93 ± 0.07	0.90 ± 0.09	0.81 ± 0.12	.0091†‡
Inferior parietal, Lt	0.94 ± 0.08	0.96 ± 0.10	0.86 ± 0.13	.0158†‡
Caudate, Lt	0.83 ± 0.08	0.91 ± 0.13	0.93 ± 0.10	.0176*
Caudate, Rt	0.80 ± 0.10	0.89 ± 0.13	0.91 ± 0.10	.0106*

Abbreviations: FDG, fluorodeoxyglucose; PET, positron emission tomography; MT subtype, medial temporal subtype; D subtype, diffuse atrophy subtype; P subtype, parietal-dominant subtype; SD, standard deviation; ICV, intracranial volume; FDR, false discovery rate; Lt, left; Rt, right.

NOTE. For each variable, the mean and standard deviation, as well as the *P* value of between-group comparisons, are shown. Age, gender, education, and ICV were treated as covariates.

*FDR corrected $P < .05$ between MT subtype and D subtype.

†FDR corrected $P < .05$ between MT subtype and P subtype.

‡FDR corrected $P < .05$ between D subtype and P subtype.

4. Discussion

The main findings of our present study are as follows: (1) cluster analysis of a multicenter international data set based on cortical atrophy patterns groups AD subjects into two subtypes (MT, D, and P); (2) the areas of glucose hypometabolism match well with the regions of cortical atrophy, whereas Aβ accumulation is predominant in the P subtype; (3) some parts of neuropsychological test results were indicative of cortical thinning patterns; and (4) neither CSF Aβ nor p-tau differ among the subgroups.

4.1. Structural MRI and clinical findings in three AD subgroups

The three subtypes of AD revealed by our cluster analysis showed different patterns of glucose hypometabolism and Aβ accumulation (sections 4.2. and 4.3.). Intriguingly, these results reflected a recent autopsy report on the pathologic classification of AD into three subtypes based on the distribution and density of neurofibrillary tangles [6]. In that report, the neurofibrillary tangle pathology groupings were 14% with limbic predominant AD, 75% with typical AD, and 11% with hippocampal sparing AD, similar to the MT, D, and P subtypes in our present study. In that previous autopsy study also, hippocampal sparing AD (homologous to the P subtype in this study) had the most severe cortical atrophy and limbic predominant AD (homologous to the MT subtype in this study) had the most severe MT lobe atrophy. In addition, limbic predominant type patients were older, more likely to be women, and prone to harbor the APOE4 allele. On the other hand, the hippocampal sparing AD cases tended to be younger at

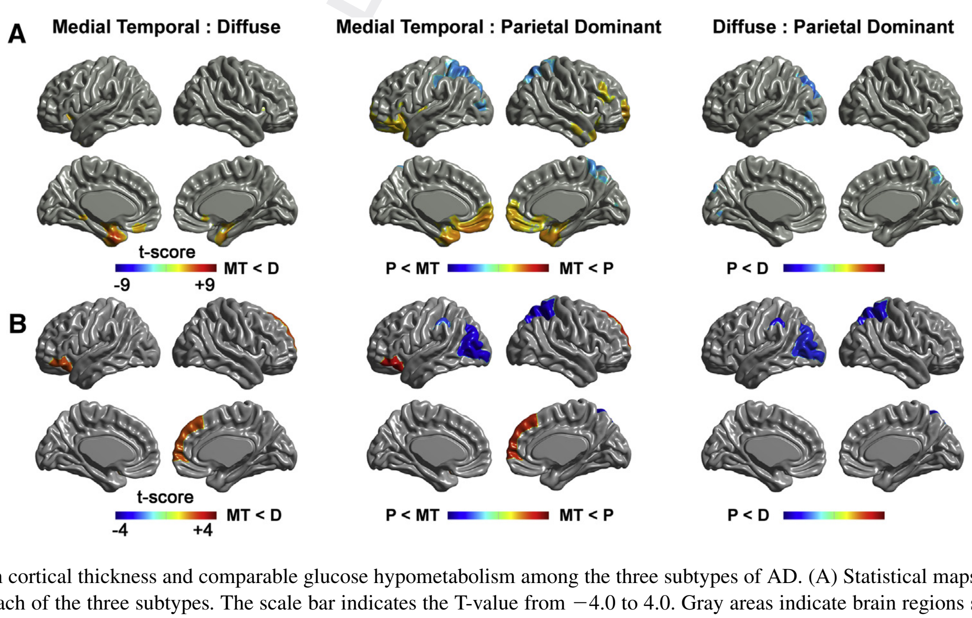

Fig. 2. Differences in cortical thickness and comparable glucose hypometabolism among the three subtypes of AD. (A) Statistical maps of cortical thickness patterns comparing each of the three subtypes. The scale bar indicates the T-value from −4.0 to 4.0. Gray areas indicate brain regions showing no statistical significance in cortical thickness compared with normal control groups. (B) Statistical maps representing the differences in glucose metabolism (FDG-PET) between each of the three subgroups. Maps at FDR corrected $P < .05$ were shown with age, sex, education, and intracranial volume serving as covariates. Abbreviations: AD, Alzheimer's disease; FDG, fluorodeoxyglucose; PET, positron emission tomography.

Table 3
Amyloid-β deposition of each region of interest of Florbetapir-PET

	MT subtype (n = 15)	D subtype (n = 43)	P subtype (n = 19)	
Region of interest	Mean ± SD	Mean ± SD	Mean ± SD	Adjusted *P*
Precentral, Lt	1.26 ± 0.18	1.22 ± 0.15	1.33 ± 0.16	.0464*
Precentral, Rt	1.31 ± 0.18	1.26 ± 0.14	1.38 ± 0.15	.0225*
Superior frontal, Lt	1.36 ± 0.22	1.29 ± 0.17	1.45 ± 0.17	.0271*
Superior frontal, Rt	1.44 ± 0.24	1.35 ± 0.18	1.54 ± 0.18	.0138*
Superior orbital frontal, Lt	1.42 ± 0.22	1.35 ± 0.18	1.52 ± 0.15	.022*
Superior orbital frontal, Rt	1.43 ± 0.23	1.36 ± 0.18	1.53 ± 0.16	.0248*
Middle frontal, Lt	1.54 ± 0.27	1.43 ± 0.23	1.64 ± 0.19	.0213*
Middle frontal, Rt	1.56 ± 0.27	1.45 ± 0.24	1.67 ± 0.19	.0259*
Middle orbital frontal, Lt	1.47 ± 0.23	1.40 ± 0.18	1.58 ± 0.16	.0457*
Middle orbital frontal, Rt	1.47 ± 0.25	1.39 ± 0.18	1.56 ± 0.16	.0479*
Inferior frontal opercular, Rt	1.49 ± 0.24	1.41 ± 0.19	1.59 ± 0.15	.0342*
Inferior frontal triangular, Rt	1.55 ± 0.26	1.46 ± 0.19	1.65 ± 0.18	.0487*
Inferior frontal orbital, Rt	1.50 ± 0.24	1.41 ± 0.18	1.60 ± 0.16	.0245*
Supplementary motor, Lt	1.48 ± 0.24	1.36 ± 0.18	1.57 ± 0.18	.0049*
Supplementary motor, Rt	1.47 ± 0.25	1.32 ± 0.18	1.53 ± 0.20	.0042†*
Superior medial frontal, Lt	1.51 ± 0.31	1.38 ± 0.23	1.60 ± 0.20	.0429*
Median cingulum, Lt	1.50 ± 0.27	1.39 ± 0.20	1.58 ± 0.22	.0182*
Median cingulum, Rt	1.48 ± 0.26	1.36 ± 0.21	1.53 ± 0.22	.0393*
Calcarine, Rt	1.56 ± 0.21	1.48 ± 0.18	1.61 ± 0.17	.045*
Fusiform, Rt	1.52 ± 0.24	1.44 ± 0.18	1.60 ± 0.17	.0405*
Postcentral, Lt	1.48 ± 0.26	1.36 ± 0.17	1.56 ± 0.19	.0038*
Postcentral, Rt	1.48 ± 0.25	1.36 ± 0.19	1.56 ± 0.20	.011*
Superior parietal, Lt	1.53 ± 0.27	1.39 ± 0.20	1.60 ± 0.23	.0072*
Superior parietal, Rt	1.50 ± 0.25	1.36 ± 0.20	1.51 ± 0.18	.0312*
Inferior parietal, Lt	1.56 ± 0.28	1.44 ± 0.20	1.64 ± 0.22	.0359*
Inferior parietal, Rt	1.57 ± 0.28	1.43 ± 0.21	1.62 ± 0.19	.0286*
Supramarginal, Rt	1.64 ± 0.27	1.54 ± 0.20	1.73 ± 0.21	.0414*
Angular, Rt	1.65 ± 0.28	1.53 ± 0.21	1.74 ± 0.20	.0203*
Precuneus, Lt	1.66 ± 0.31	1.49 ± 0.21	1.72 ± 0.28	.0076†*
Precuneus, Rt	1.62 ± 0.29	1.47 ± 0.21	1.67 ± 0.25	.0191*
Paracentral lobule, Lt	1.42 ± 0.22	1.34 ± 0.15	1.52 ± 0.20	.0048*
Paracentral lobule, Rt	1.41 ± 0.22	1.35 ± 0.15	1.51 ± 0.18	.0248*

Abbreviations: MT subtype, medial temporal subtype; D subtype, diffuse atrophy subtype; P subtype, parietal-dominant subtype; SD, standard deviation; PET, positron emission tomography; FDR, false discovery rate; Lt, left; Rt, right; ICV, intracranial volume.

NOTE. For each variable, the mean and standard deviation, as well as the *P* value of between-group comparisons, are shown. Age, gender, education, and ICV were treated as covariates.

*FDR corrected $P < .05$ between MT subtype and D subtype.

†FDR corrected $P < .05$ between D subtype and P subtype.

symptom onset and have a shorter disease duration, a faster disease course, and more atypical and nonamnestic presentation than the other subtypes.

In our present study, the P subtype cases were also younger at symptom onset than those of the MT or D subtypes, which finding is consistent with hippocampus-sparing AD. Given the fact that the global cognitive assessments did not differ among these three subgroups (Table 1), the younger age in the P subtype subjects may suggest a faster disease course [7]. There were some discrepancies

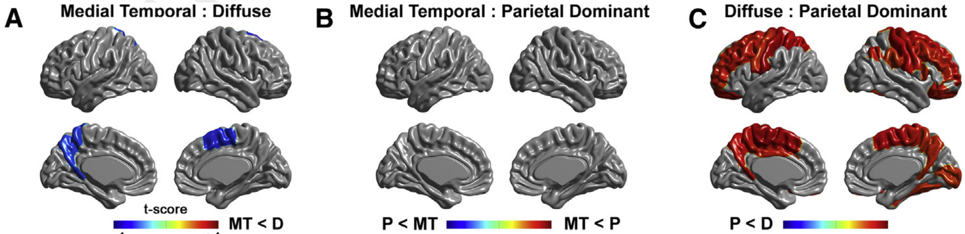

Fig. 3. Prominent deposition of fibrillary forms of amyloid-beta (Florbetapir-PET) in the brains of the parietal dominant AD subtype. Maps at FDR corrected $P < .05$ were shown with age, sex, education, and intracranial volume serving as covariates. Abbreviations: AD, Alzheimer's disease; PET, positron emission tomography; FDR, false discovery rate.

Table 4
Neuropsychological test results

	MT subtype (n = 15)	D subtype (n = 43)	P subtype (n = 19)		
	Mean ± SD	Mean ± SD	Mean ± SD	*P*	Adjusted *P*
Clock drawing*	3.33 ± 1.63	3.44 ± 1.42	2.84 ± 1.50	.3316	.4446
Clock copy*	4.60 ± 0.83	4.47 ± 0.74	3.63 ± 1.71	.0819	.1352
BNT	20.47 ± 5.90	22.53 ± 5.68	25.00 ± 4.29	.0560	.2391
RAVLT trial (sum of five trials)	19.80 ± 5.44	25.07 ± 8.32	21.84 ± 7.09	.0492	.0714
RAVLT 30-min delay*	0.33 ± 0.62	1.02 ± 1.93	0.63 ± 1.38	.5413	.4788
RAVLT recognition	7.20 ± 3.80	7.49 ± 3.81	6.11 ± 3.00	.3849	.4170
Logical memory, immediate	3.60 ± 3.14	5.07 ± 2.74	3.95 ± 2.46	.1293	.2401
Logical memory, delayed*	0.87 ± 1.41	2.00 ± 2.16	1.68 ± 2.11	.2117	.2122
Category fluency (animals)	11.67 ± 4.27	13.09 ± 5.55	11.42 ± 3.67	.3846	.3636
TMT A-time to complete	55.07 ± 28.39	58.95 ± 34.22	80.67 ± 39.46	.0541	.0412[†‡]
TMT B-time to complete	198.86 ± 88.07	160.92 ± 80.09	194.82 ± 69.80	.2235	.1785
ADNI-MEM	−0.80 ± 0.41	−0.44 ± 0.44	−0.68 ± 0.43	.0116[§]	.0237[§]
ADNI-EF	−0.75 ± 0.86	−0.55 ± 0.89	−1.07 ± 0.71	.0844	.0679
Interlocking pentagon, n (%)	13 (86.7)	38 (88.4)	4 (21.1)	<.0001[†‡]	.001[†‡]

Abbreviations: MT subtype, medial temporal subtype; D subtype, diffuse atrophy subtype; P subtype, parietal-dominant subtype; SD, standard deviation; BNT, Boston naming test; RAVLT, Rey's auditory vocabulary list test; TMT, trail making test; ADNI-MEM, Alzheimer's Disease Neuroimaging Initiative memory composite score; ADNI-EF, Alzheimer's Disease Neuroimaging Initiative executive functioning composite score; FDR, false discovery rate; ICV, intracranial volume.

NOTE. Age, gender, education, and ICV were treated as covariates.

*Kruskal-Wallis test was done.

[†]FDR corrected $P < .05$ between MT subtype and P subtype.

[‡]FDR corrected $P < .05$ between D subtype and P subtype.

[§]FDR corrected $P < .05$ between MT subtype and D subtype.

between our findings and those of the autopsy study. For example, the male predominance in the hippocampal sparing AD group and the APOE4 allele preference in the limbic predominant group were not noted in our P or MT subtypes, respectively. This may be due to the relatively small number of subjects assessed in our present analyses. However, similar to the autopsy study, we found no significant differences between the P, MT, and D patients in terms of education level, cognitive performance, or daily activities measured by MMSE, CDR, CDR-SB, ADAS-Cog 11, ADAS-Cog 13, MoCA, and GDepS, thereby suggesting that our subgroups had a similar disease status and were well matched for comparison (Table 1). When we additionally assessed detailed neuropsychological tests, we found the MT subtype showed less performance in memory tests and the P subtype scored less in the interlocking pentagon test, which suggest that the cortical thinning patterns reflect cognitive changes at least in part. Taken together, we conclude that clustering according to cortical atrophy patterns on MRI is comparable with grouping based on the pathologic subtypes of AD.

4.2. *Glucose hypometabolism comparable with cortical atrophy*

The FDG-PET image findings in our study potentially reflected the AD pathologies in the brain. FDG-PET, a marker of synaptic activity and neuronal functioning, is known to correlate well with tau accumulation or neuronal and synaptic injuries in the brain [20–22]. At the same time, glucose hypometabolism is indicative of neurodegeneration and structural changes in MRI [23–26]. Areas of hypometabolism noted in each subtype in our present study matched well with regions of cortical atrophy (Table 2 and Fig. 2). Patients in the P subtype showed glucose hypometabolism in the right superior, left inferior parietal, and left middle occipital cortices. This is consistent with previous study results showing glucose hypometabolism in the parietal lobes in patients with EOAD compared with late-onset Alzheimer's disease (LOAD) patients [8,27]. Interestingly, patients in the MT subtype in our current series showed glucose hypometabolism in the left hippocampus. As the MT lobe is the most vulnerable area to tau accumulation and subsequent neurodegeneration, the glucose hypometabolism and cortical atrophy in these lobes in the MT subtype may be indicative of the limbic predominant AD reported in the autopsy study [28,29].

In terms of the progression of the tau pathology (neurofibrillary tangles) in the brain, previous studies suggest that neurofibrillary tangles begin to accumulate in the MT lobes, including the transentorhinal cortex, and then spread to the posterior temporal lobes and parietal lobes, finally evolving to the frontal lobes [30]. It has been further suggested that this pattern of spread matches well with future brain atrophy [31]. As FDG-PET results can reflect tau-mediated injury and both FDG-PET and tau are markers of neurodegeneration [24,32], the three subtypes noted in our current analyses may include information on pathologically defined subtypes based on neurofibrillary tangles.

4.3. Prominent amyloid uptake in the P subtype

In our Florbetapir-PET analysis, patients in the P subtype showed marked Aβ accumulation in most brain regions compared with that in the MT and D subtypes. Recent advances in the understanding of preclinical AD indicate that Aβ builds up rapidly and almost plateaus before the onset of clinical symptoms of AD [33]. Many experimental and clinical studies have demonstrated that Aβ accumulation precedes tau-mediated neuronal injury and glucose hypometabolism [24,34,35]. At the same time, the extent of tau pathology but not Aβ burden is known to correlate with the rate of atrophy in AD [4]. The lack of difference in amyloid uptake between the MT and D subtypes, but not in glucose hypometabolism or cortical atrophy patterns, may also stem from the fact that Aβ builds up preclinically and reaches its maximal level by the time of clinical symptom development. Because patients in the P subtype were younger and had a similar degree of global cognitive function at the time of PET imaging, they may have an earlier Aβ accumulation and faster disease course. These findings are in line with a previous study that compared the amyloid PET findings between EOAD and LOAD patients and demonstrated marked amyloid uptakes in the cortices of EOAD subjects [36].

4.4. No difference in CSF Aβ and tau among the subtypes

In our present study, the CSF results showed no significant differences among the P, MT, and D subtypes. Because changes in the CSF Aβ levels are known to precede the fibrillar forms of amyloid noted by amyloid PET, as well as FDG-PET and structural MRI changes, any differences in CSF Aβ among the three groups would have been diminished at the time of assessment [32]. Moreover, because the CSF obtained by lumbar puncture would yield pooled information on tau or Aβ in the whole brain, it may have less temporal or regional resolution than PET or structural MRI.

Correlations between glucose hypometabolism, impaired cognition, and high CSF tau levels have been demonstrated [37]. On the other hand, there are other evidences showing that cortical atrophy on MRI would be a later event in AD progression, preceded by changes in CSF tau and FDG-PET [24]. Based on these findings, and because our current subjects were all demented at the time of assessment, the differences in CSF tau would have been diminished. Relatively small number of subjects investigated in this study would have affected the lack of difference among the groups.

There were several limitations of our present study of note. First, without autopsy findings we could not confirm whether the regional distribution of glucose hypometabolism measured by FDG-PET directly reflected the regional distribution of neurofibrillary tangles. This will need to be confirmed in subsequent studies using tau or neuroinflammation images. Second, there were some demographic discrepancies between our findings and the results from the autopsy study. This was due in part to the relatively small number of subjects we analyzed. We hope to address whether the differences in cortical thickness can also indicate demographic differences among the P, MT, and D subgroups in a future study with a larger sample size. The prevalence of TDP 43 pathology is known to be high in limbic predominant AD and affects the clinical manifestations of AD [38,39]. By excluding subjects with hippocampal sclerosis and TDP 43, previous autopsy studies have tried to specifically address neurofibrillary tangle pathology, which is not possible in an MRI-based study [6,38,39]. Therefore, our three subtypes classified by MRI cortical thickness patterns potentially included TDP 43 or hippocampal sclerosis pathologies in the brain. This would have contributed to discrepancies in the clinical characteristics among our three subgroups. Finally, brain atrophy in our AD subjects potentially affected the PET findings. Using partial volume correction in both sets of PET analyses, we tried to eliminate the possibility of an underestimation in glucose hypometabolism or amyloid uptake in regions with marked atrophy [17].

The AD subtypes described in our present study may suggest different patterns of disease progression and responses to treatment. Consideration of these three patterns of brain cortical atrophy will potentially be important when estimating the prognosis of AD and in planning treatment strategies in a clinical setting. Future studies supported by pathologic findings or tau imaging will enable further understanding of the regional and temporal relationships between the main pathophysiological manifestations of AD, including neurofibrillary tangle accumulation and cortical atrophies.

Acknowledgments

Data collection and sharing for this project was funded by the Alzheimer's Disease Neuroimaging Initiative (ADNI) (National Institutes of Health grant U01 AG024904) and DOD ADNI (Department of Defense award number W81XWH-12-2-0012). ADNI is funded by the National Institute on Aging, the National Institute of Biomedical Imaging and Bioengineering, and through generous contributions from the following: Alzheimer's Association; Alzheimer's Drug Discovery Foundation; Araclon Biotech; BioClinica, Inc.; Biogen Idec; Bristol-Myers Squibb Company; Eisai; Elan Pharmaceuticals, Inc.; Eli Lilly and Company; EuroImmun; F. Hoffmann-La Roche Ltd. and its affiliated company Genentech, Inc.; Fujirebio; GE Healthcare; IXICOLtd.; Janssen Alzheimer Immunotherapy Research & Development, LLC.; Johnson & Johnson Pharmaceutical Research & Development LLC.; Medpace; Merck & Co., Inc.; Meso Scale Diagnostics, LLC.; NeuroRx Research; Neurotrack Technologies; Novartis Pharmaceuticals Corporation; Pfizer Inc.; Piramal Imaging; Servier; Synarc; and Takeda Pharmaceutical Company. The Canadian Institutes of Health Research is providing funds to support ADNI clinical sites in Canada. Private sector contributions are facilitated by the Foundation for the National Institutes of Health (www.fnih.org). The grantee organization is the Northern California Institute for Research and Education, and the study is coordinated by the Alzheimer's Disease Cooperative Study at the University of California, San Diego. ADNI data are disseminated by the Laboratory for Neuro Imaging at the University of Southern California.

This work was supported by the Basic Science Research Program through the National Research Foundation of Korea (NRF) funded by the Ministry of Science, ICT and Future Planning (2013R1A1A1012925), a grant of the Korea Health Technology R&D Project through the Korea Health Industry Development Institute (KHIDI), funded by the Ministry of Health & Welfare, Republic of Korea (grant number: HI14C3319), a grant from the Korea Institute of Science and Technology Institutional Open Research Program (2E24242-13-110), and grants (2015-590; 2014-0783) from the Asan Institute for Life Sciences (J.H.R.).

Supplementary data

Supplementary data related to this article can be found at http://dx.doi.org/10.1016/j.dadm.2015.11.008.

RESEARCH IN CONTEXT

1. Systematic review: We investigated whether a cortical thickness–based clustering method would reflect pathologically defined subtypes of Alzheimer's disease (AD). After clustering of 77 AD subjects from the Alzheimer's Disease Neuroimaging Initiative 2 data set, biomarker findings were compared among the groups.
2. Interpretation: Three cortical thinning patterns were noted: medial temporal (MT; 19.5%), diffuse (55.8%), and parietal dominant (P; 24.7%) atrophy subtypes. The P subtype was the youngest and represented more glucose hypometabolism in the parietal and occipital cortices and marked amyloid-beta accumulation in most brain regions. The MT subtype revealed more glucose hypometabolism in the left hippocampus and bilateral frontal cortices. These findings suggest cortical thickness patterns can indeed reflect pathophysiological changes in AD.
3. Future directions: Given the easy accessibility of magnetic resonance imaging, our findings have advanced the AD field with imaging-based expectations of pathophysiology, disease progression, and responses to treatment in AD. Future studies supported by pathologic findings will enable further understanding of our results.

References

[1] Duyckaerts C, Braak H, Brion JP, Buee L, Del Tredici K, Goedert M, et al. PART is part of Alzheimer disease. Acta Neuropathol 2015; 129:749–56.
[2] Price JL, Morris JC. Tangles and plaques in nondemented aging and "preclinical" Alzheimer's disease. Ann Neurol 1999;45:358–68.
[3] Price JL, Morris JC. So what if tangles precede plaques? Neurobiol Aging 2004;25:721–3. discussion 43–6.
[4] Josephs KA, Whitwell JL, Ahmed Z, Shiung MM, Weigand SD, Knopman DS, et al. Beta-amyloid burden is not associated with rates of brain atrophy. Ann Neurol 2008;63:204–12.
[5] Silbert LC, Quinn JF, Moore MM, Corbridge E, Ball MJ, Murdoch G, et al. Changes in premorbid brain volume predict Alzheimer's disease pathology. Neurology 2003;61:487–92.
[6] Murray ME, Graff-Radford NR, Ross OA, Petersen RC, Duara R, Dickson DW. Neuropathologically defined subtypes of Alzheimer's disease with distinct clinical characteristics: A retrospective study. Lancet Neurol 2011;10:785–96.
[7] Whitwell JL, Dickson DW, Murray ME, Weigand SD, Tosakulwong N, Senjem ML, et al. Neuroimaging correlates of pathologically defined subtypes of Alzheimer's disease: A case-control study. Lancet Neurol 2012;11:868–77.
[8] Noh Y, Jeon S, Lee JM, Seo SW, Kim GH, Cho H, et al. Anatomical heterogeneity of Alzheimer disease: Based on cortical thickness on MRIs. Neurology 2014;83:1936–44.
[9] Seo SW, Im K, Lee JM, Kim ST, Ahn HJ, Go SM, et al. Effects of demographic factors on cortical thickness in Alzheimer's disease. Neurobiol Aging 2011;32:200–9.
[10] Collins DL, Neelin P, Peters TM, Evans AC. Automatic 3D intersubject registration of MR volumetric data in standardized Talairach space. J Comput Assist Tomogr 1994;18:192–205.
[11] Sled JG, Zijdenbos AP, Evans AC. A nonparametric method for automatic correction of intensity nonuniformity in MRI data. IEEE Trans Med Imaging 1998;17:87–97.
[12] Zijdenbos AP, Forghani R, Evans AC. Automatic "pipeline" analysis of 3-D MRI data for clinical trials: Application to multiple sclerosis. IEEE Trans Med Imaging 2002;21:1280–91.
[13] Kim JS, Singh V, Lee JK, Lerch J, Ad-Dab'bagh Y, MacDonald D, et al. Automated 3-D extraction and evaluation of the inner and outer cortical surfaces using a Laplacian map and partial volume effect classification. Neuroimage 2005;27:210–21.
[14] Lerch JP, Evans AC. Cortical thickness analysis examined through power analysis and a population simulation. Neuroimage 2005; 24:163–73.
[15] Whitwell JL, Przybelski SA, Weigand SD, Ivnik RJ, Vemuri P, Gunter JL, et al. Distinct anatomical subtypes of the behavioural variant of frontotemporal dementia: A cluster analysis study. Brain 2009;132:2932–46.
[16] Johnson RA, Wichern DW. Applied multivariate statistical analysis. Englewood Cliffs, N.J: Prentice-Hall; 1982.
[17] Musiek ES, Chen Y, Korczykowski M, Saboury B, Martinez PM, Reddin JS, et al. Direct comparison of fluorodeoxyglucose positron emission tomography and arterial spin labeling magnetic resonance imaging in Alzheimer's disease. Alzheimers Dement 2012;8:51–9.
[18] Shaw LM, Vanderstichele H, Knapik-Czajka M, Clark CM, Aisen PS, Petersen RC, et al. Cerebrospinal fluid biomarker signature in Alzheimer's disease neuroimaging initiative subjects. Ann Neurol 2009; 65:403–13.
[19] Genovese CR, Lazar NA, Nichols T. Thresholding of statistical maps in functional neuroimaging using the false discovery rate. Neuroimage 2002;15:870–8.
[20] Sokoloff L. Relationships among local functional activity, energy metabolism, and blood flow in the central nervous system. Fed Proc 1981;40:2311–6.

[21] Schwartz WJ, Smith CB, Davidsen L, Savaki H, Sokoloff L, Mata M, et al. Metabolic mapping of functional activity in the hypothalamo-neurohypophysial system of the rat. Science 1979;205:723–5.

[22] Attwell D, Laughlin SB. An energy budget for signaling in the grey matter of the brain. J Cereb Blood Flow Metab 2001;21:1133–45.

[23] Adriaanse SM, van Dijk KR, Ossenkoppele R, Reuter M, Tolboom N, Zwan MD, et al. The effect of amyloid pathology and glucose metabolism on cortical volume loss over time in Alzheimer's disease. Eur J Nucl Med Mol Imaging 2014;41:1190–8.

[24] Jack CR Jr, Knopman DS, Jagust WJ, Shaw LM, Aisen PS, Weiner MW, et al. Hypothetical model of dynamic biomarkers of the Alzheimer's pathological cascade. Lancet Neurol 2010;9:119–28.

[25] Chetelat G, Desgranges B, Landeau B, Mezenge F, Poline JB, de la Sayette V, et al. Direct voxel-based comparison between grey matter hypometabolism and atrophy in Alzheimer's disease. Brain 2008; 131:60–71.

[26] Bokde AL, Pietrini P, Ibanez V, Furey ML, Alexander GE, Graff-Radford NR, et al. The effect of brain atrophy on cerebral hypometabolism in the visual variant of Alzheimer disease. Arch Neurol 2001; 58:480–6.

[27] Ossenkoppele R, Zwan MD, Tolboom N, van Assema DM, Adriaanse SF, Kloet RW, et al. Amyloid burden and metabolic function in early-onset Alzheimer's disease: Parietal lobe involvement. Brain 2012;135:2115–25.

[28] Landau SM, Harvey D, Madison CM, Koeppe RA, Reiman EM, Foster NL, et al. Associations between cognitive, functional, and FDG-PET measures of decline in AD and MCI. Neurobiol Aging 2011;32:1207–18.

[29] Landau SM, Mintun MA, Joshi AD, Koeppe RA, Petersen RC, Aisen PS, et al. Amyloid deposition, hypometabolism, and longitudinal cognitive decline. Ann Neurol 2012;72:578–86.

[30] Braak H, Braak E. Neuropathological stageing of Alzheimer-related changes. Acta Neuropathol 1991;82:239–59.

[31] Whitwell JL. Progression of atrophy in Alzheimer's disease and related disorders. Neurotox Res 2010;18:339–46.

[32] Jack CR Jr, Knopman DS, Jagust WJ, Petersen RC, Weiner MW, Aisen PS, et al. Tracking pathophysiological processes in Alzheimer's disease: An updated hypothetical model of dynamic biomarkers. Lancet Neurol 2013;12:207–16.

[33] Jack CR Jr, Lowe VJ, Weigand SD, Wiste HJ, Senjem ML, Knopman DS, et al. Serial PIB and MRI in normal, mild cognitive impairment and Alzheimer's disease: Implications for sequence of pathological events in Alzheimer's disease. Brain 2009;132:1355–65.

[34] Meyer-Luehmann M, Spires-Jones TL, Prada C, Garcia-Alloza M, de Calignon A, Rozkalne A, et al. Rapid appearance and local toxicity of amyloid-beta plaques in a mouse model of Alzheimer's disease. Nature 2008;451:720–4.

[35] Benzinger TL, Blazey T, Jack CR Jr, Koeppe RA, Su Y, Xiong C, et al. Regional variability of imaging biomarkers in autosomal dominant Alzheimer's disease. Proc Natl Acad Sci U S A 2013;110:E4502–9.

[36] Cho H, Seo SW, Kim JH, Suh MK, Lee JH, Choe YS, et al. Amyloid deposition in early onset versus late onset Alzheimer's disease. J Alzheimers Dis 2013;35:813–21.

[37] Petrie EC, Cross DJ, Galasko D, Schellenberg GD, Raskind MA, Peskind ER, et al. Preclinical evidence of Alzheimer changes: Convergent cerebrospinal fluid biomarker and fluorodeoxyglucose positron emission tomography findings. Arch Neurol 2009;66:632–7.

[38] Crane PK, Carle A, Gibbons LE, Insel P, Mackin RS, Gross A, et al. Development and assessment of a composite score for memory in the Alzheimer's Disease Neuroimaging Initiative (ADNI). Brain Imaging Behav 2012;6:502–16.

[39] Gibbons LE, Carle AC, Mackin RS, Harvey D, Mukherjee S, Insel P, et al. A composite score for executive functioning, validated in Alzheimer's Disease Neuroimaging Initiative (ADNI) participants with baseline mild cognitive impairment. Brain Imaging Behav 2012; 6:517–27.